Direct control of defects in molybdenum oxide and understanding their high CO$_2$ sorption performance

Mohammad Tanhaei[1,2], Yi Ren[1], Ming Yang[1], Fabio Bussolotti[1], Jayce JW Cheng[1], Jisheng Pan[1], Sing Yang Chiam[1]*

1. Institute of Materials Research and Engineering, Agency for Science, Technology and Research, 2 Fusionopolis Way, 138634, Singapore

2. Division of Physics and Applied Physics, School of Physical and Mathematical Sciences, Nanyang Technological University, 21 Nanyang Link, Singapore 637371, Singapore

Corresponding author:

Dr. Sing Yang Chiam

Email: chiamsy@imre.a-star.edu.sg, Tel/Fax: (+65) 64168964

CO₂ sorption performance from current literature

Table S1: Sorption capacity of different materials for CO_2 with their synthesis method

Material	Synthesis Method	Structure	Sorption capacity (mmol/g)	Test Condition	Reference
TiO_2 @Zeolite	MLD[1]	Pellet	1.62	0.5 bar 25 °C	[15]
PEI[2] @ PME[3]	Impregnation	Powder	7.31	400 ppm CO_2 25 °C	[16]
MgO(111)	Aero-gel methodology	Powder	1.28	1 atm 35 °C	[35]
$Li_{4+x}Si_{1-x}Fe_xO_4$	Ball Milling	Powder	2.5	200 °C	[16]
MgO	Flame aerosol	Nanoparticle	1.5	60 °C	[17]
Li_6WO_6	Solid-state reaction	Nanowire	2.7	710 °C 60 s	[14]
NCC-AO[4]	EISA[5]	Nanocrystalline	3.30 5.54	25 °C, 1 atm 120 °C	[18]
$MgO-SiO_2$ $CaO-SiO_2$	Sol-gel	Composites	2.61 4.71	25 °C, 1 atm 120 °C	[15]

1 = Molecular Layer Deposition
2 = Polyethylenimine
3 = Extralarge-pore silica (pore-expanded MCM-41)
4 = nanocrystalline cellulose (NCC)–mesoporous silica composites (NCC-AO) with attached double-amidoxime
5 = evaporation-induced self-assembly

Table S1 shows the different CO_2 sorption materials from literature. The highest performing results stands at ~7.31mmol/g while more typical values ranges more from 1-5.5 mmol/g. All of the reported work uses powder or nanoparticle as the platform for adsorption.

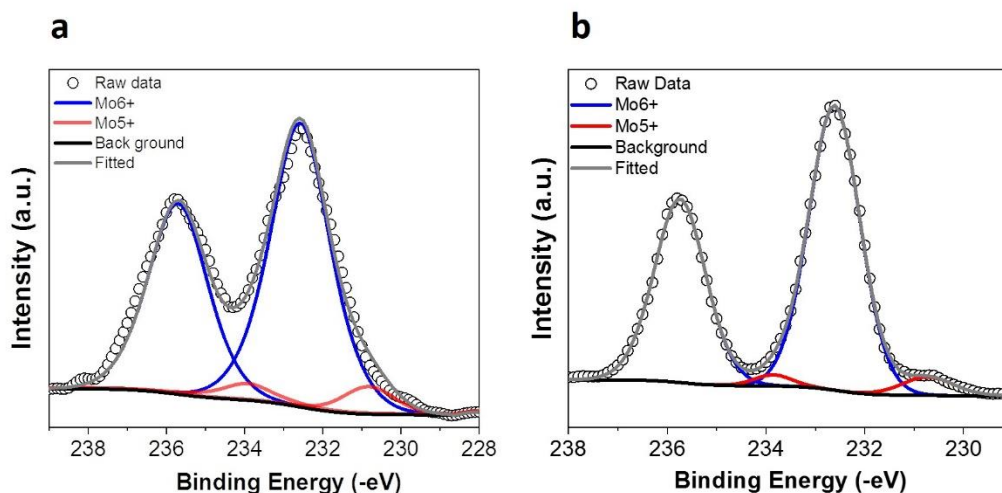# XPS of near stoichiometry samples

Figure S1. The Mo 3d core-level photoelectron spectra for electrodeposited Mo oxide film on (a) Al substrate after oxidation in ambient at 500°C; (b) cleaned ITO substrate.

Figure S1 shows the Mo 3d core-level photoelectron spectra for electrodeposited Mo oxide film on Al substrate after oxidation in ambient at 500°C, and on cleaned ITO substrate. The ITO substrate was cleaned in ultrasonic bath with acetone, isopropanol (IPA) and deionized water each for 5 mins before electrodeposition. The Mo 3d core-level peaks are fitted with contributions from mostly Mo^{6+}, with a small shoulder of Mo^{5+}. It is also noted that the full-width half maximum (FWHM) of the oxidized Al is larger due to lower conductivity, as compared with the highly conductive ITO. Both figures show low defect contribution for electroplating on a high oxygen content surface.
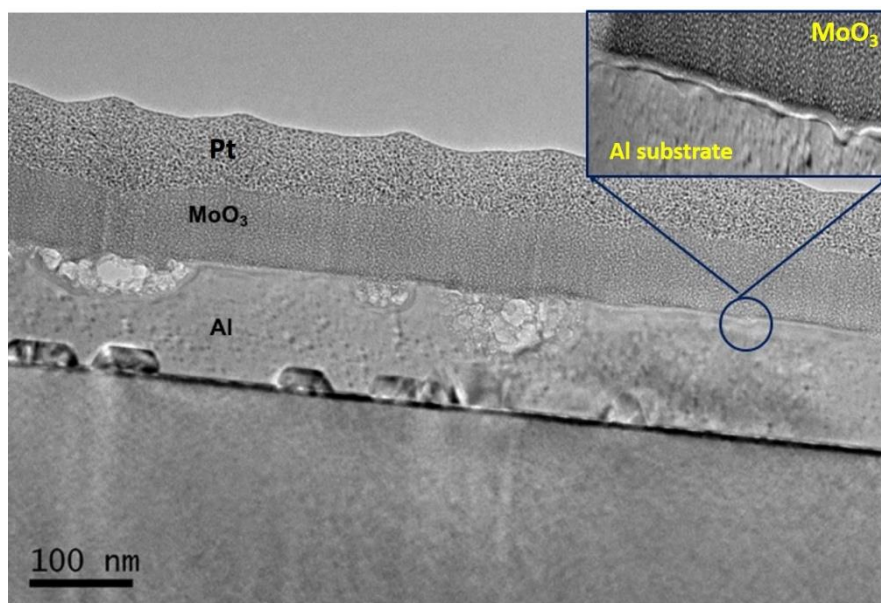
Cross-section micrographs of MoO$_3$

Figure S2. Cross-section TEM image of the electrodeposited molybdenum oxide film on the aluminum.

Figure S2 shows the cross section transmission electron microscopy (TEM) image of the electrodeposited Mo oxide on Al coated Si. Pure Aluminum is evaporated on the silicon substrate and used as a working electrode for the electrodeposition that was performed under identical conditions. The Si substrate was used to obtain higher quality cross-sectional imaging of the deposited films for thickness evaluations. A larger magnification of the micrograph at the interface is also shown in the inset. Typical thickness of the film measured is around 80 nm.

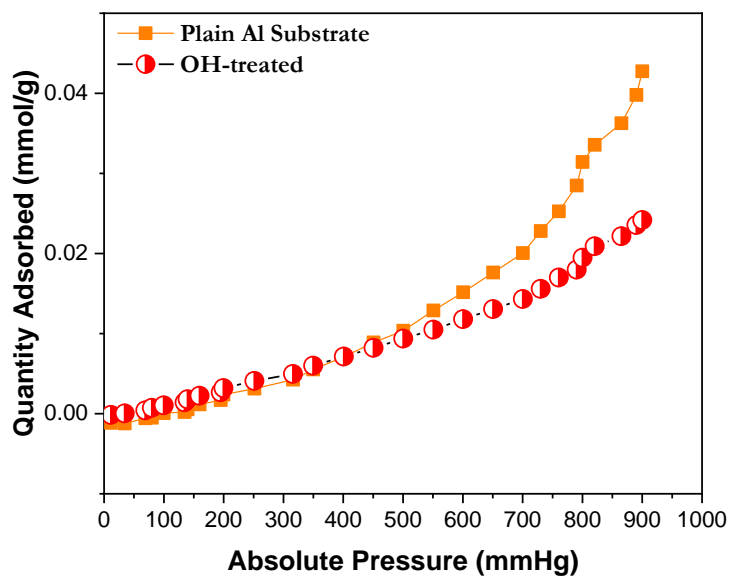# Sorption performance of plain aluminum substrate

Figure S3. Sorption isotherm for the plain and OH- treated Aluminum substrate.

The sorption isotherm for the bare and OH- treated Aluminum (Al) substrate is shown in Figure S3. This shows the sorption performance of a bare Al sample. To calculate the absolute sorption quantities of the Mo oxide film, the isotherms of the plain Al substrate are subtracted from the coated samples, before multiplying by the measured weight of the samples.

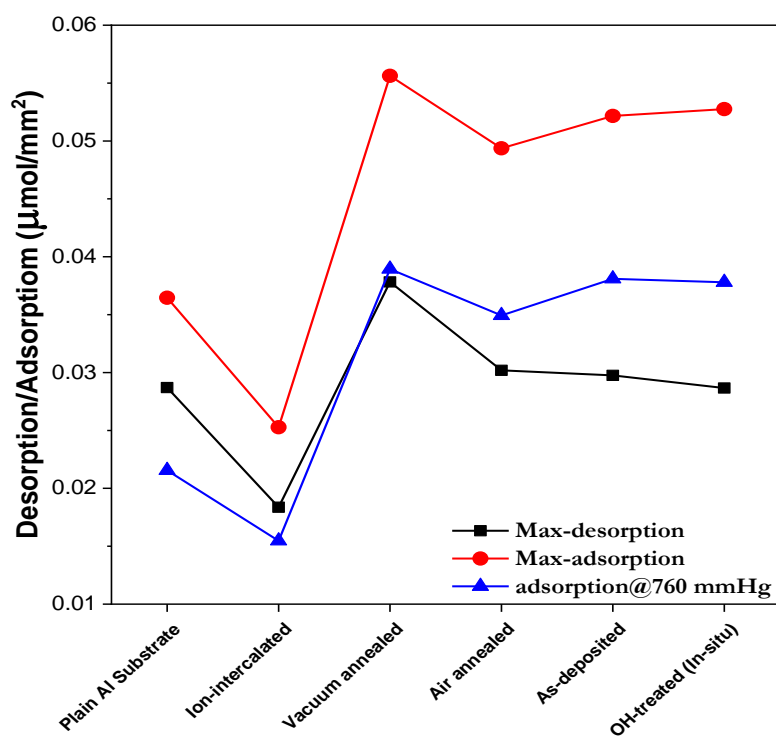# Desorption performance for the different films

Figure S4. Desorption performance for the various samples tested.

The desorption performance for the various sample is shown in Fig. S4 with the data given in the Table S2 below. The maximum desorption is taken from the difference of the maximum absorption, from the reading at 100 mmHg, representing desorption with pressure swing. In general, the samples with higher Mo^{4+} defects showed lower % of desorption. The desorption percentage is similar to reported values in the literature at around 20-40% [1-4].

Table S2 Desorption performance with pressure swing

| Sample	Max-Desorption ($\mu mol/mm^2$)	Max-Adsorption ($\mu mol/mm^2$)	% of Desorption
Plain Al Substrate	0.0287	0.03646	21.67
Ion-intercalated	0.01837	0.02528	27.33
Vacuum annealed	0.03782	0.05563	32.01
Air annealed	0.03019	0.04937	38.85
As-deposited	0.02976	0.05216	42.94
OH-treated (In-situ)	0.02866	0.05275	45.67

[1] Gunathilake, Chamila, and Mietek Jaroniec. "Mesoporous calcium oxide–silica and magnesium oxide–silica composites for CO 2 capture at ambient and elevated temperatures." *Journal of Materials Chemistry A* 4.28 (2016): 10914-10924.

[2] Hahn, Maximilian W., et al. "Mechanism and kinetics of CO2 adsorption on surface bonded amines." *The Journal of Physical Chemistry C* 119.8 (2015): 4126-4135.

[3] Goeppert, Alain, et al. "Easily regenerable solid adsorbents based on polyamines for carbon dioxide capture from the air." *ChemSusChem* 7.5 (2014): 1386-1397.

[4] Uehara, Yusuke, Davood Karami, and Nader Mahinpey. "Effect of Water Vapor on CO2 Sorption–Desorption Behaviors of Supported Amino Acid Ionic Liquid Sorbents on Porous Microspheres." *Industrial & Engineering Chemistry Research* 56.48 (2017): 14316-14323

Calculation to demonstration performance of sorption coatings
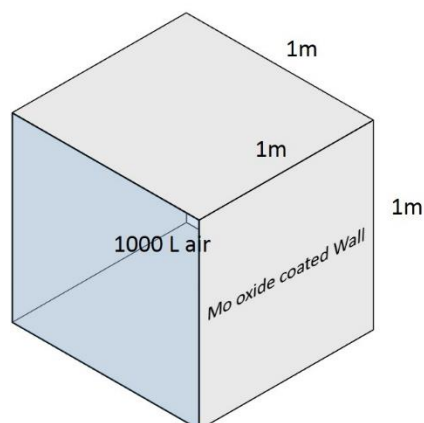
If we apply ideal-gas law to the air:

at standard pressure (P=1 atm) and temperature (T=298 K), 1000L of air (1m^3 room) equal to:

$$n = \frac{PV}{RT} = \frac{1\,atm \times 1000l}{0.082 \frac{lit.\,atm}{mol.\,k} \times 298k} = 40.89 \text{ mol air } (N_2 + O_2)$$

If we assume: $400\ ppm = 0.04\%\ CO_2\ in\ air$

$$CO_2 = \frac{0.04}{100} \times 40.89 = 0.0163\ mol\ CO_2\ gas$$

So, the room should have about **0.0163** mol CO_2

Figure S5. Illustrations and calculations of CO_2 sorption in a 1 m^3 enclosed room

Figure S5 shows an illustration and calculation used to estimate sorption potential of the coatings. At 0.018 µmol/mm^2, this translates to 0.018 mol/m^2. In a 1 m^3 room at room temperature, using N_2 and O_2 as the bulk number of molecules in the room, calculations yielded approximately 0.016 mol of CO_2. Therefore, a single sided fully coated wall will be sufficient, capacity wise, to remove the total amount of CO_2 in the room.
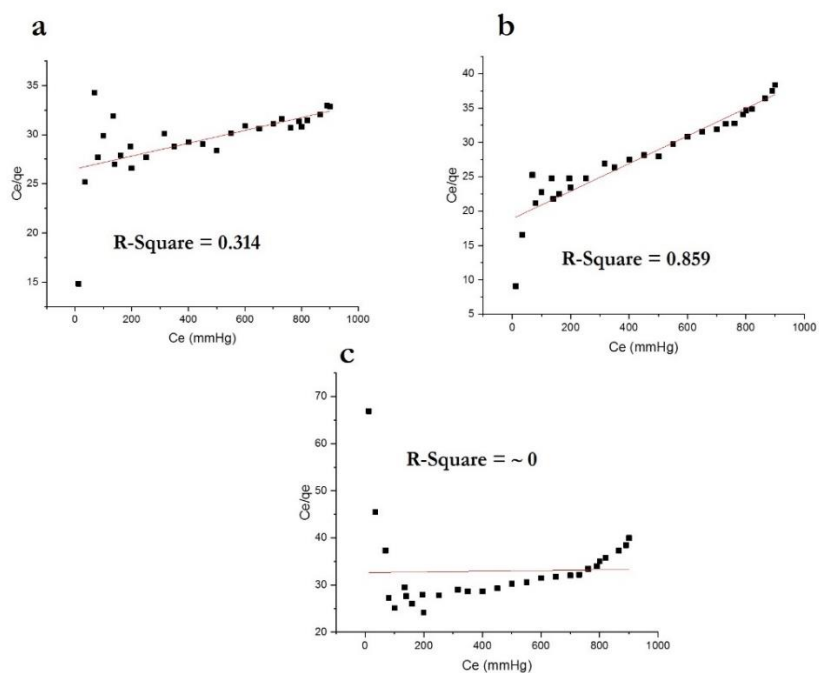
Fittings of isotherms

Figure S6. Langmuir model and indicated fitted R-square values for the: a) Vacuum annealed, b) As-deposited, and c) OH-treated samples.
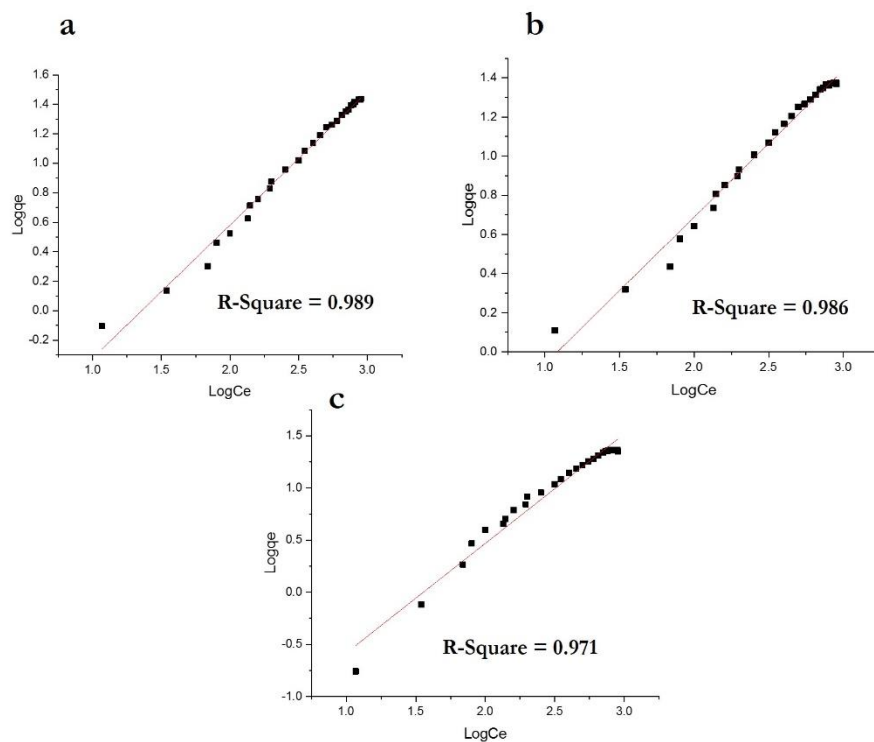

Figure S7. Freundlich model and indicated fitted R-square values for the: a) Vacuum annealed, b) As-deposited, and c) OH-treated samples.

Langmuir (L) and Freundlich (F) isotherm models are separately fitted for different samples and results are shown in Figure S6 and S7. Correlation coefficient (R^2) value for L model are poor, while there is a better fit with the F model showing that the sorption follows more closely with a system of distributed sorption sites of different affinities. Subsequent fitting with the L-F model shows excellent fit for CO_2 sorption with R^2 values of >0.99 (Figure 4 in manuscript), showing also some limited homogeneous interactions at higher adsorbate concentration. [1,2]

[1] Jeppu, Gautham P., and T. Prabhakar Clement. "A modified Langmuir-Freundlich isotherm model for simulating pH-dependent adsorption effects." Journal of contaminant hydrology 129 (2012): 46-53.

[2] Ayawei, Nimibofa, Augustus Newton Ebelegi, and Donbebe Wankasi. "Modelling and interpretation of adsorption isotherms." Journal of Chemistry 2017 (2017).
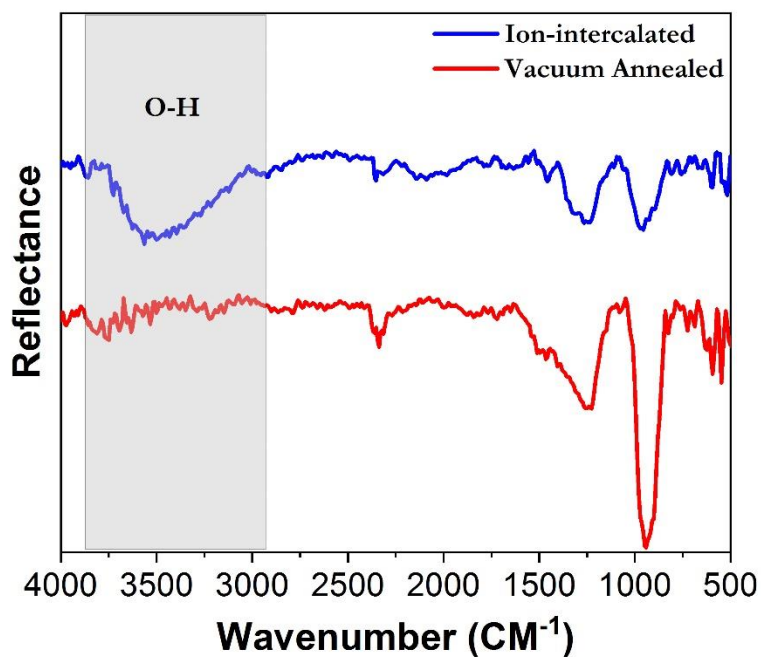
FTIR data showing hydroxyl content

Figure S8. FT-IR spectra for the vacuum annealed and ion-intercalated Mo oxide thin films.

The FT-IR spectra for the ion-intercalated sample shows higher OH$^-$ content around wavenumber of 3560 cm^{-1} [1] as highlighted in Figure S8. Electrodeposition, and/or electrochemical cycling in acidic solutions can lead to presence of hydroxyls. We believe this is the main reason for the sorption performance of the ion-intercalated sample.

[1] Upadhyay, Kush K., et al. "Electrodeposited MoOx films as negative electrode materials for redox supercapacitors." Electrochimica Acta 225 (2017): 19-28.

DFT calculations

All the DFT calculations were performed using Vienna Ab-initio Simulation Package (VASP.5.4.4) [1-2] with local density approximation (LDA) for the exchange-correlation functional and the projector-augmented-wave (PAW) method.[3] The cut-off energy was set to 500 eV, and the energy and force was converged to 10^{-5} eV and 0.01 eV/Å, respectively. For the orthorhombic MoO_3 bulk, a 12×10×4 k-point mesh was adopted for the first-Brillouin zone sampling. Based on these settings, the calculated lattice constants of the MoO_3 bulk are a=3.74, b=3.77, and c=13.71 Å, comparable to the reported experimental values and previous calculations [4-6]. The LDA functionals were used in this study because they are appealing for systems with significant multi-configurational wave function character such as transition metal oxide catalysts due to their cost advantages [7]. We also used PBE functionals with the van der Waals correction (DFT-D3) to calculate the adsorption energy [8]. As Figure S9 shows, the trend of the adsorption energy for CO_2 on the MoO_3 surface with the defects are consistent with LDA results. In this study, the effective Hubbard U=6.3 has been applied on Mo d orbital because previous study suggested that this value can give a reaction energy for $MoO_3 \rightarrow MoO_2 + 1/2O_2$ comparable with experimental value [9].

We simulated a CO_2 molecule adsorbed on the surface of 3×3×1 pristine MoO_3 (001) supercell (Mo^{6+}), and the surface with one bridge oxygen vacancy (O_{v-b}) (Mo^{5+}), with one top O_v (O_{v-t}) (Mo^{4+}), and the top O_v passivated by an OH group, as illustrated in Figure S10. In the simulation, a vacuum layer thicker than 15 Å was applied normal to MoO_3 surface, and the corresponding Brillouin zones were sampled by using 4×4×1 k-point mesh. During the structural optimization, the bottom two MoO_3 layers were fixed. We also applied dipole correction to minimize the artificial dipole potential [10]. The adsorption energy and charge redistribution for the CO_2 molecule on the MoO_3 surfaces were calculated by:

$$E_a = E_{CO_2+MoO_3} - E_{CO_2} - E_{MoO_3}$$

and

$$\Delta\rho = \rho_{CO_2+MoO_3} - \rho_{CO_2} - \rho_{MoO_3}$$

where $E_{CO_2+MoO_3}$ and $\rho_{CO_2+MoO_3}$ are total energy and charge density of CO_2 adsorbed on the MoO_3 surface, and E_{CO_2} (ρ_{CO_2}) and E_{MoO_3} (ρ_{MoO_3}) are the total energy (charge density) of the isolated CO_2 molecule and the MoO_3 surface. Here, a more negative adsorption energy indicates stronger adsorption.
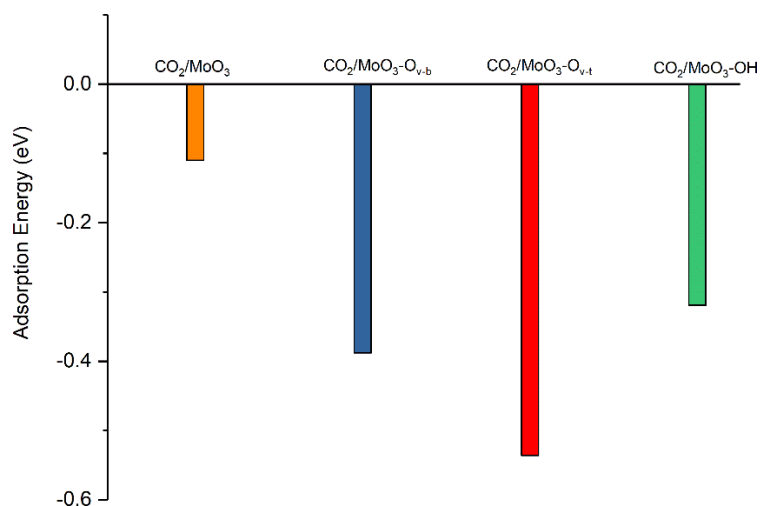

Figure S9. The PBE functionals calculated adsorption energy of CO_2 on the MoO_3 surface (CO_2/MoO_3) with the surface oxygen at the bridge site (CO_2/MoO_3-O_{v-b}), at the top site (CO_2/MoO_3-O_{v-t}), and the oxygen vacancy at the top passivated by an OH group (CO_2/MoO_3).
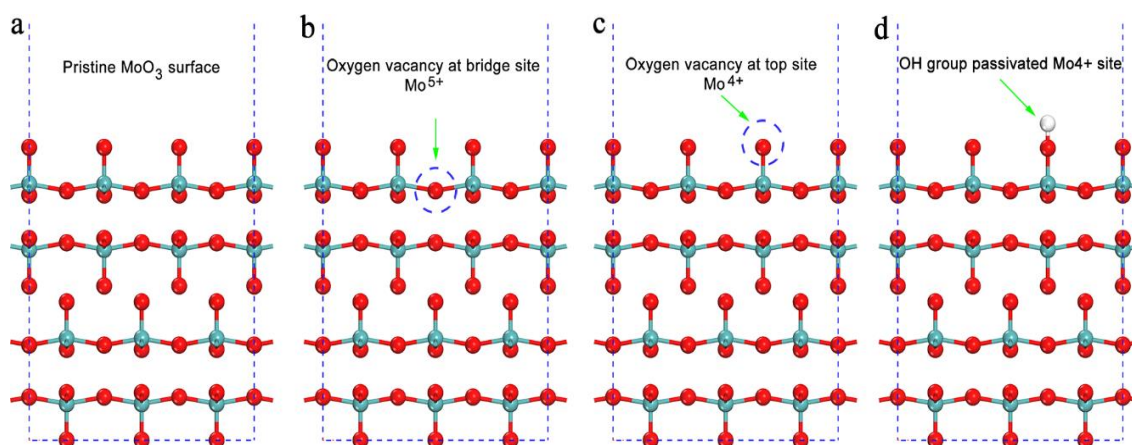

Figure S10. An illustration of atomic structures (side view) of (a) pristine MoO_3 (001) surface, and the surface with (b) an oxygen vacancy at the bridge site (c), top site and (d) the top site oxygen vacancy passivated by an OH group. The dashed blue circle denotes the oxygen vacancy.

Figure S10 shows the stable configuration of surface defects in this study. Figure S10a represents a pristine stoichiometry MoO_3 (001) surface, which represents a Mo^{6+} configuration. Figure S10b illustrates an oxygen vacancy at the bridge site, which introduces Mo^{5+} defect states at the surface. Figure S10c illustrates an oxygen vacancy at the top site, which produces Mo^{4+} defect states at the surface. Finally, Figure S10d illustrates a configuration whereby the oxygen vacancy at the top site was passivated by an OH group. The corresponding top view of the adsorption configuration is shown in Figure S11.
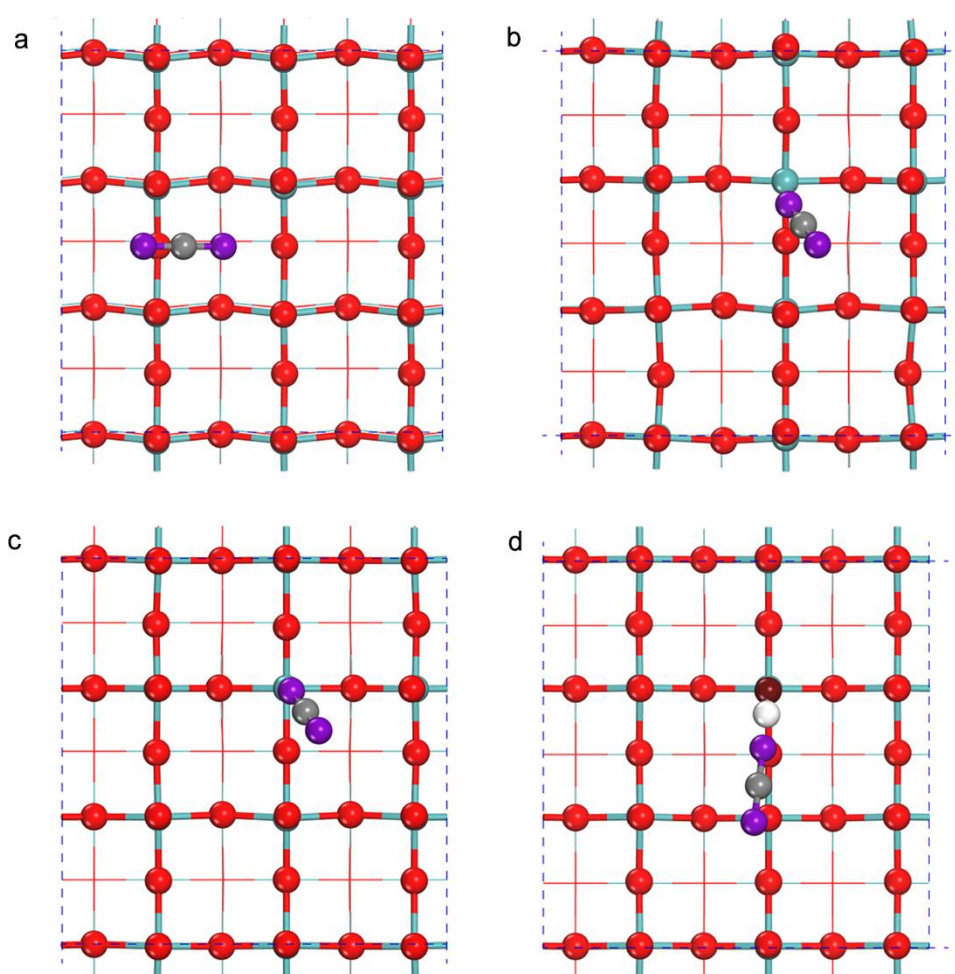

Figure S11. The adsorption configuration (top view) of CO_2 on (a) pristine MoO_3 surface, (b) MoO_3 with a Mo^{4+} defect, (c) MoO_3 with Mo^{5+} defect and (d) MoO_3 with a Mo^{4+} defect passivated by an OH group, in which the purple solid dots and dark red dots denote the oxygen atom in CO_2 molecular and OH group, respectively.
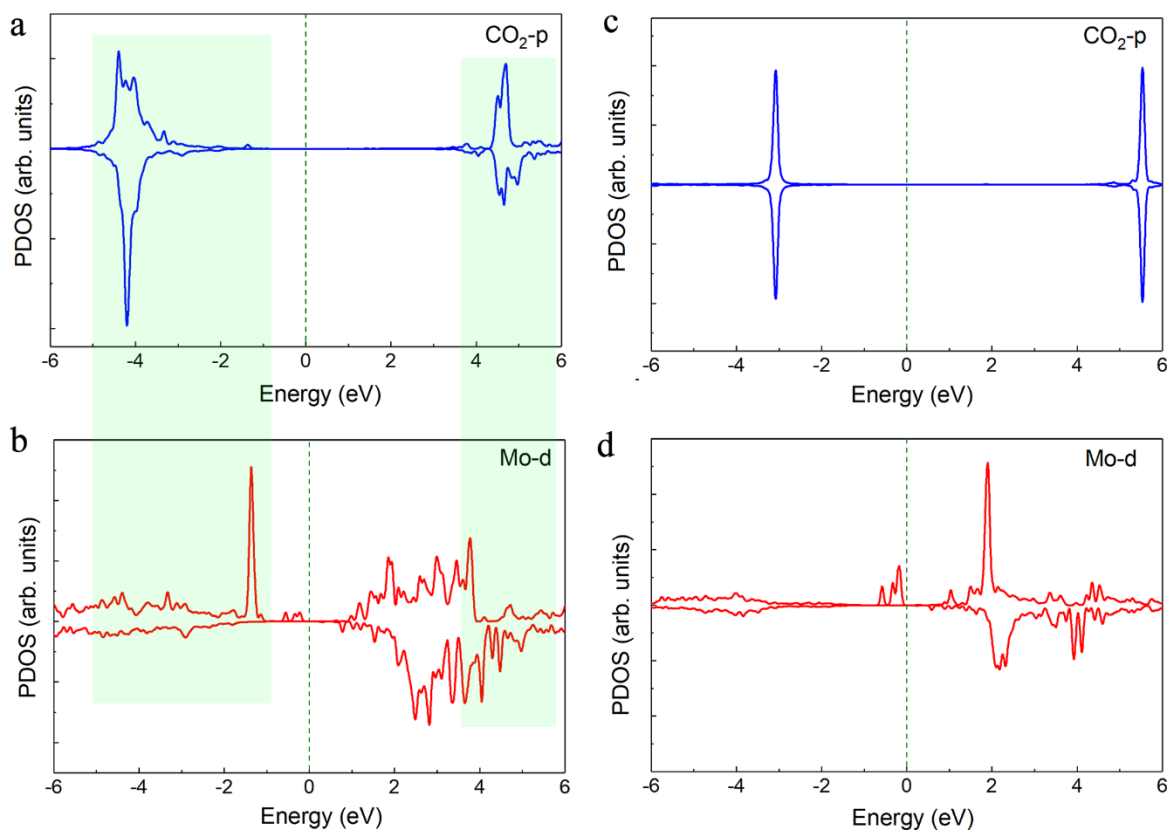
Figure S12. The projected density of states on CO_2 molecule (a) and its nearest Mo atom (b) for the CO_2 adsorbed on the MoO_3 surface with an oxygen vacancy at the top site. The projected density of states on CO_2 molecule (c) and its nearest Mo atom (d) for the CO_2 adsorbed on the MoO_3 surface with an OH group passivated top-site oxygen vacancy. Fermi level is shifted to 0 eV.

Figure S12a and b show the projected density of states (PDOSs) on the p orbital of the CO_2 molecule and the d orbital of its nearest Mo atom for the CO_2 molecule adsorbed on the MoO_3 surface with an oxygen vacancy at the top site (Mo^{4+} defect). These PDOSs further indicate the stronger interaction between Mo^{4+} defect state and CO_2. The weaker occupied states near Fermi level projected in Mo d orbital infer the stronger charge transfer from the Mo d into the CO_2 p orbital, thus resulting in similar PDOSs between the CO_2 and the Mo^{4+} states. From the PDOSs, a stronger orbital hybridization between Mo d orbital and CO_2 p orbital is noticeable. In contrast, if the Mo^{4+} defect was passivated

by an OH group, the interaction between the CO_2 molecule and the MoO_3 surface becomes much weaker, resulting in the two very different PDOSs as shown in Figure S10c and d.

Reference:

[1] Kresse, G.; Furthmüller, J. Efficient iterative schemes for ab initio total-energy calculations using a plane-wave basis set. Phys. Rev. B 1996, 54, 11169.

[2] Kresse, G.; Joubert, D. From ultrasoft pseudopotentials to the projector augmented-wave method. Phys. Rev. B 1999, 59, 1758.

[3] Perdew, J. P.; Burke, K.; Ernzerhof, M. Generalized gradient approximation made simple. Phys. Rev. Lett. 1996, 77, 3865.

[4] Lei, Y.; Chen, Z. DFT+U Study of Properties of MoO3 and Hydrogen Adsorption on $MoO_3(010)$. J. Phys. Chem. C 2012, 116, 25757−25764.

[5] Negishi, H.; Negishi, S.; Kuroiwa, Y.; Sato, N.; Aoyagi, S. Anisotropic Thermal Expansion of Layered MoO_3 Crystals. Phys. Rev. B 2004, 69, 064111.

[6] Head, A. R.; Tsyshevsky, R.; Trotochaud, L.; Yu, Y.; Kyhl, L.; Karshoğlu, O.; Kuklja, M. M.; Bluhm, H. Adsorption of Dimethyl Methylphosphonate on MoO_3: The Role of Oxygen Vacancies. J. Phys. Chem. C 2016, 120, 29077−29088.

[7] Peverati, R.; Truhlar, D. M11-L: A Local Density Functional That Provides Improved Accuracy for Electronic Structure Calculations in Chemistry and Physics, J. Phys. Chem. Lett. 2012, 3, 1, 117–124.

[8] Grimme, S.; Ehrlich, S.; Goerigk, L. Effect of the Damping Function in Dispersion Corrected Density Functional Theory, J. Comp. Chem. 2011, 32, 1456-1465.

[9] Lei, Yan-Hua, and Zhao-Xu Chen. "DFT+ U study of properties of MoO3 and hydrogen adsorption on MoO3 (010)." The Journal of Physical Chemistry C 116.49 (2012): 25757-25764.

[10] Neugebauer, J.; Scheffler, M. Adsorbate-Substrate and Adsorbate-Adsorbate Interactions of Na and K Adlayers on Al(111), Phys. Rev. B 1992, 46, 1606.